

# Flow and structure of fluids in functionalized nanopores

José Rafael Bordin\*

*Campus Caçapava do Sul, Universidade Federal do Pampa,  
Av. Pedro Anunciação, 111, CEP 96570-000, Caçapava do Sul, RS, Brazil*

Marcia C. Barbosa†

*Instituto de Física, Universidade Federal do Rio Grande do Sul,  
Caixa Postal 15051, CEP 91501-970, Porto Alegre, RS, Brazil*

## Abstract

We investigate through non-equilibrium Molecular Dynamics simulations the structure and flow of fluids in functionalized nanopores. The nanopores are modeled as cylindrical structures with solvophilic and solvophobic sites. Two fluids are modeled. The first is a standard Lennard Jones fluid. The second one is modeled with a isotropic two-length scale potential, which exhibits in bulk water-like anomalies. Our results indicates distinct dependence of the overall mass flux for each species of fluid with the number of solvophilic sites for different nanotubes radii. Also, the density and fluid structure are dependent from the nanotube radius and the solvophilic properties of the nanotube. This indicates that the presence of a second length scale in the fluid-fluid interaction will lead to distinct behavior. Also, our results shows that chemically functionalized nanotubes with different radius will have distinct nano-fluidic features. Our results are explained in the basis of the characteristic scale fluid properties and the effects of nanoconfinement.

---

\* josebordin@unipampa.edu.br

† marcia.barbosa@ufrgs.br

## I. INTRODUCTION

Most liquids contract upon cooling at constant pressure and diffuse slower upon compression. This is not the case of a wide range of materials that expand as the temperature is decreased and move faster as the pressure grows. Liquid water is the most known of this anomalous materials [1] but it is not the only one. The maximum in the diffusion coefficient at constant temperature was observed in water [2] but also in silicon [3] and silica [4]. The maximum in the density is present in water [5] but also in silicon [4], silica [6], Te [7], Bi [8], Si [9],  $Ge_{15}Te_{85}$  [10], liquid metals [11], graphite [12] and  $BeF_2$  [13].

The origin of the unusual behavior observed in anomalous materials is the presence of two characteristics length scales. While non anomalous liquids can be described on the framework of the van der Waals one length scale potential, anomalous materials exhibit two characteristic scales. Then it became natural to associate the thermodynamic and dynamic anomalous behavior of these materials with a core-softened (CS) potentials with two length scales (TLS) in the bulk [14–19] or under confinement [20–26].

Recently a new puzzle was added to list of anomalous behaviors of water. Experiments and simulations show that the mobility of water through nanotubes membranes exceeds the values calculated from continuum hydrodynamics models by more than three orders of magnitude [27–33]. This behavior is also observed in non anomalous materials such as ionic liquids [34], hydrogen, methane, nitrogen, air, of oxygen, of argon [35, 36]. In this case, however, the fast flow exceeds predictions by only one order of magnitude [27, 28]. Naturally, two questions arise: what is the mechanism behind the fast flow in nanoconfinement and why in the case of water it is much faster.

In the particular case of water, the hydrophobicity adds up to this already complex problem [37, 38]. While for the hydrophobic wall-water interaction in an homogeneous tube the flow is faster than in the pure hydrophilic wall-water interaction [39, 40], for an heterogeneous wall-water system the flow is faster as the system becomes fully hydrophilic [37, 41].

The existence of confining structures in which hydrophobic and hydrophilic sites are present is not just a theoretical assumption. Recent methods allowed the synthesis of nanotubes similar to CNTs, as Boron-Nitride nanotubed (BNNTs) [42] and carbon doped BNNTs [43]. Chemically functionalized nanotubes can have hydrophobic and hydrophilic sites, similar to biological channels, witch have distinct solvophobic properties depending on the

forming amino acids. Also, gas adsorption and storage in doped and chemically treated nanotubes have been recently investigated [44, 45]. Therefore studying these systems is not only a theoretical challenge but it has realistic applications.

In this paper we explore the differences and similarities between the anomalous and non anomalous fluids flow by computer simulations. We compute the mobility of a water-like system under solvophilic, solvophobic and mixed confinement. This behavior is then compared with the flow of a non anomalous, standard LJ fluid also confined within an attractive, a repulsive and a mixed walls. Our results aim to shade some light in the controversial results both in the water-like and non anomalous confinement in the different types of wall-fluid interactions.

The paper is organized as follows: in Sec. II we introduce the model and describe the methods and simulation details; the results are given and discussed in Sec. III; and in Sec. IV we present our conclusions.

## II. MODEL AND SIMULATIONAL DETAILS

In this paper all physical quantities are computed in the standard Lennard-Jones (LJ) units [46], as instance

$$r^* \equiv \frac{r}{\sigma}, \quad \rho^* \equiv \rho\sigma^3, \quad \text{and} \quad t^* \equiv t \left( \frac{\epsilon}{m\sigma^2} \right)^{1/2}, \quad (1)$$

for distance, density of particles and time, respectively, where  $\sigma$  is the distance parameter,  $\epsilon$  the energy parameter and  $m$  the mass parameter. Since all physical quantities are defined in reduced LJ units, the  $*$  is omitted, in order to simplify the discussion.

Two types of fluids are analyzed: a water-like fluid and a non anomalous fluid. Both are modeled by coarse-graining potentials. The water-like system is represented by a two length scale interaction potential and the non anomalous fluid is depicted by an one length scale interaction potential. In both cases the system is modeled by spherical particles with effective diameter  $\sigma$  and mass  $m$ . The water-like particles interact through the three dimensional core-softened potential (TLS):

$$U_{ij}^{\text{TLS}}(r_{ij}) = \epsilon' \left[ \left( \frac{\sigma}{r_{ij}} \right)^{12} - \left( \frac{\sigma}{r_{ij}} \right)^6 \right] + \sum_{i=1}^3 \frac{B_i}{B_i^2 + (r_{ij} - C_i)^2}, \quad (2)$$

where  $r_{ij} = |\vec{r}_i - \vec{r}_j|$  is the distance between fluid particles  $i$  and  $j$ . The first term on the right is the standard 12-6 LJ potential [46], while the second term corresponds to Lorentzian

distributions centered at  $C_i$  with amplitude  $1/B_i$ . In this paper, the potential parameter are:  $k = 3$ ,  $\epsilon' = 0.6$ ,  $B_1 = 0.3$ ,  $B_2 = -1.5$ ,  $B_3 = 2.0$ ,  $C_1 = 1.0$ ,  $C_2 = 1.8$  and  $C_3 = 3.0$ , resulting in the TLS potential showed in the figure 1. The first length scale is at  $\approx 1.0$ , the particle diameter. The second length scale is located at  $\approx 1.5$ . This type of effective potential exhibits the density, diffusion and structural anomalous behavior present in water [18] and it has been used as a coarse-graining model for system with thermodynamic, dynamic and structural anomalous behavior.

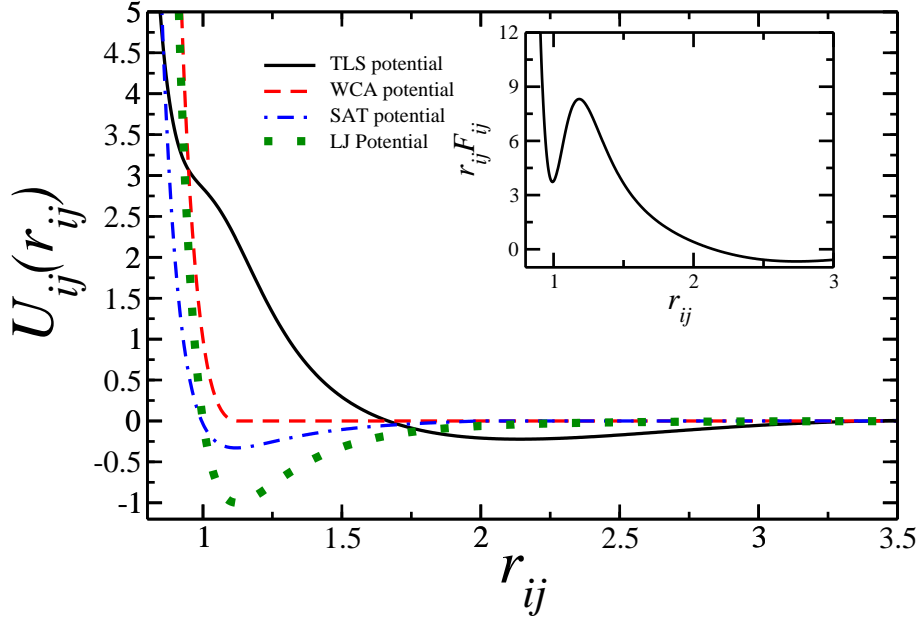


FIG. 1. Interactions potentials used in our simulations as function of particles separation  $r_{ij}$ . The solid black line is the TLS potential used to modeled the anomalous fluid. The dashed red line is the purely repulsive WCA potential, while de dot-dashed blue line is the attractive SAT potential. The dotted green line represents the LJ potential. Inset:  $r_{ij}F(r_{ij})$  versus  $r_{ij}$  for the TLS potential. According to Debenedetti *et al* [47] a potential will show anomalous behavior if there is a region where  $(\partial r_{ij}F(r_{ij})/\partial r_{ij}) > 0$ .

The non anomalous particles interact through the standard Lennard-Jones potential also shown in the fig. 1 and given by,

$$U_{LJ}(r_{ij}) = 4\epsilon \left[ \left( \frac{\sigma}{r_{ij}} \right)^{12} - \left( \frac{\sigma}{r_{ij}} \right)^6 \right], \quad (3)$$

where  $\epsilon$  is the depth of the attractive well. The LJ potential is showed as the green dotted line in figure 1. This potential has been used to model simple one length scale system in

which the density, diffusion and structural anomalous behavior observed in water is not seen. Here the system is analyzed in the pressure-temperature region in which no liquid-gas phase transition is present.

We explore the behavior of these two types of fluids confined inside a cylindrical nanopore. In order to observe the flow, the nanotube is connected to two reservoirs, namely, CV<sub>1</sub> on the left of the nanopore and CV<sub>2</sub> at the right, as depicted in the figure 2. The simulation box is a parallelepiped with dimensions  $5L \times L \times L$  in  $xyz$  directions, with  $L = 16$ . The tube structure is built as a wrapped sheet of spherical particles with diameter  $\sigma_{\text{NT}} = \sigma$ . Each particle in the nanotube represents a site that interacts with the fluid by an attractive or a repulsive that in the case of interaction with water are called solvophilic or solvophobic interactions. For simplicity even when interacting with the LJ fluid these attractive and repulsive interactions will be called solvophilic and solvophobic. Solvophobic sites and fluid particles interact through the purely repulsive Weeks-Chandler-Andersen (WCA) potential [46] given by

$$U_{ij}^{\text{WCA}}(r_{ij}) = \begin{cases} U_{\text{LJ}}(r_{ij}) - U_{\text{LJ}}(r_c), & r_{ij} \leq r_c, \\ 0, & r_{ij} > r_c, \end{cases} \quad (4)$$

where  $r_{ij}$  is the distance between the fluid particle  $i$  and the nanopore particle  $j$ ,  $r_c = 2^{1/6}\sigma$  and  $\epsilon' = 4.0$ . Solvophilic sites and fluids interact with the fluid through the strong attractive (SAT) potential [22] namely

$$U_{ij}^{\text{SAT}}(r_{ij}) = \begin{cases} D_1 \left[ \left( \frac{\sigma}{r_{ij}} \right)^{12} - \left( \frac{\sigma}{r_{ij}} \right)^6 \right] + D_2 \left[ \frac{r_{ij}}{\sigma} \right] - \epsilon_{\text{SAT}}, & r_{ij} \leq r_c, \\ 0, & r_{ij} > r_c, \end{cases} \quad (5)$$

where  $r_{ij}$  is the distance between the fluid particle  $i$  and the nanopore particle  $j$ ,  $D_1 = 1.2$ ,  $D_2 = 0.0545$ ,  $\epsilon_{\text{SAT}} = D_1[(1/r_c)^{12} - (1/r_c)^6] + D_2[r_c]$  and  $r_c = 2.0$ .

Here we explore three cases: systems with solvophobic, solvophilic and mixed nanotube. The three cases are represented by the fraction of solvophilic sites,  $\phi$ , defined as the number of solvophilic particles in the nanopore structure divided by the total number of particles in the nanopore structure. The figure 2 illustrates nanopores fully solvophobic,  $\phi = 0.0$ , half solvophobic,  $\phi = 0.5$ , and completely solvophilic,  $\phi = 1.0$ . The solvophilic sites are placed starting at the left extrema of the nanopore, in contact with the CV<sub>1</sub> reservoir, until the desired fraction  $\phi$ . The nanotube entrances are surrounded by flat walls, which also interact with the fluid particles through the WCA potential. To avoid the flux between the CV<sub>1</sub>

and  $CV_2$  due the periodic boundary condition, flat walls are placed in the extrema of the simulation box in the  $x$  direction. These walls also interact with the fluid particles through the WCA potential.

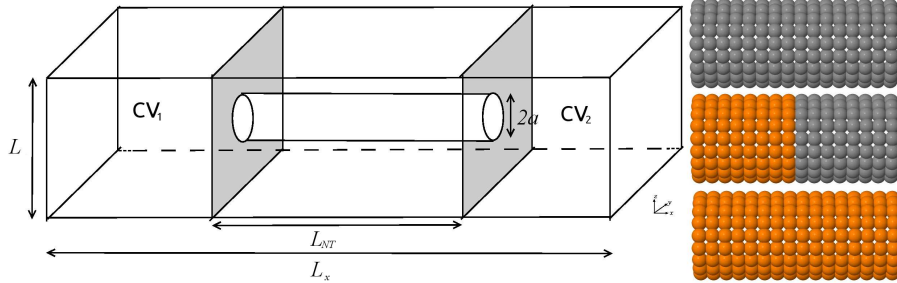


FIG. 2. Left: Schematic depiction of the simulation box. The system is composed of a high density reservoir, namely  $CV_1$ , and a low density reservoir,  $CV_2$ , connected by a nanopore. Flat and repulsive walls surround each entrance of the nanopore. The cylindrical pore in the center has radius  $a$  and length  $L_{NT}$ . Right: gray spheres represents solvophobic sites and orange spheres represents solvophilic sites in the nanopore. From up to down we can see a completely solvophobic nanopore ( $\phi = 0.0$ ), a half-solvophilic half-solvophobic nanopore ( $\phi = 0.5$ ) and a completely solvophilic nanopore ( $\phi = 1.0$ ).

The temperature of the system was fixed in  $T = 0.5$  by means of the Nose-Hoover thermostat with a coupling parameter  $Q = 2$ . This temperature ensures that the bulk system is not in the solid state. For simplicity, we assume that the nanopore atoms are motionless during the entire simulation. Periodic boundary conditions are applied in the  $y$  and  $z$  directions. A time step of  $\delta t = 0.005$  was adopted.

A steady state flux through the nanopore is obtained by fixing a higher density in the reservoir  $CV_1$ ,  $\rho_1 = 0.065$ , and a lower density in  $CV_2$ ,  $\rho_2 \approx 10^{-3}$ . The initial state is generated using a standard Grand Canonical Monte Carlo (GCMC) simulation inside each reservoir, during  $5 \times 10^5$  steps, with the initial velocity for each particle obtained from a Maxwell-Boltzmann distribution at the desired temperature. The densities inside the reservoirs are maintained constant using the Dual Control Volume Grand Canonical Molecular Dynamics (DCV-GCMD) method [48, 49]. In this method, the desired densities are restored in  $CV_1$  and  $CV_2$  by intercalating the MD steps with a number of GCMC steps inside the corresponding control volumes depicted in the figure 2. In our simulations, an initial  $5 \times 10^5$

MD steps were used for equilibration of the system, and 50 GCMC steps were performed for every 150 MD steps during the DCV-GCMD process. These rate for the simulation steps ensures that the density in each reservoir changes less than 0.5%. Final results were obtained after performing a total of  $5 \times 10^6$  MD steps for each simulation, and averaging over 5 to 10 independent runs to evaluate relevant physical quantities. Error bars are not shown since they are smaller than the data point. We have studied the flow induced only by the density gradient and the flow induced by the density gradient plus a constant, external gravitational-like force to verify the effects of external fields on the flux.

The axial flux of particles through the nanopore,  $J_{x,\text{tube}}$ , is computed by counting the number of particles that cross the channel from left to right,  $n_{\text{ltr}}$ , and the particles flowing from right to left,  $n_{\text{rtl}}$  [48],

$$J_{x,\text{pore}} = \frac{n_{\text{ltr}} - n_{\text{rtl}}}{A_{\text{NT}} N_{\text{steps}} \delta t}, \quad (6)$$

where  $A_{\text{NT}} = \pi a_{\text{eff}}^2$ , with  $a_{\text{eff}} = a - \sigma$  the effective radius available for the fluid,  $N_{\text{steps}}$  is the total number of steps used in the simulation, and  $\delta t$  is the MD time step. In an entirely similar way, we evaluate the flux in the  $x$ -direction for the non-confined case,  $J_{x,\text{bulk}}$ , but now using  $A = L \times L$ , since there is no nanopore in the system. The  $J_{x,\text{bulk}}$  was used to normalize  $J_{x,\text{pore}}$  in order to compare the bulk and confined flow. Here we assume that the fluid-fluid interaction for anomalous and non anomalous fluids, Equations (2) and (3), has a cutoff radius  $r_{\text{cut}} = 3.5$ . Two nanopore radii were simulated:  $a = 1.75$  and  $a = 5.0$ . In all simulations, the tube length is fixed to  $L_{\text{NT}} = 16$ .

### III. RESULTS AND DISCUSSION

#### A. Water-like Fluid

Let us first exam what happens with the water-like fluid confined. The figure 3 illustrates the dependence of the flux of the fluid with the fraction of solvophilic sites,  $\phi$ , for two values of the nanotube diameter,  $a$ , and distinct external forces,  $f$ . The fluid flux is strongly affected by the nanopore radius. For the narrowest tube,  $a = 1.75$ , showed in the figure 3(a), the flow increases with  $\phi$  linearly until  $\phi \approx 0.5$ , and then saturates at high values of  $\phi$ . A linear fit is shown for  $\phi < 0.5$ . For the highest value of  $f$  the flow has a maximum at  $\phi \approx 0.4$ . A similar behavior was observed by Moskowitz et al. [37] in simulations of TIP3P water inside

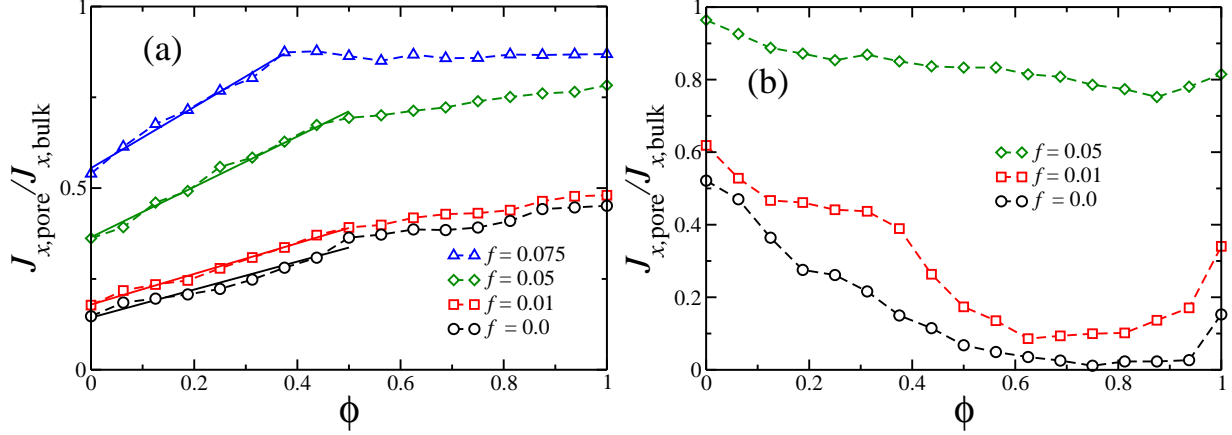


FIG. 3. Flux of anomalous particles through the nanopore,  $J_{x,pore}$ , in units of the non-confined flux,  $J_{x,bulk}$ , as function of the fraction of solvophilic sites  $\phi$  for different external forces  $f$  and for cylindrical nanopores with radius (a)  $a = 1.75$  and (b)  $a = 5.00$ .

narrow nanotubes with tunable hydrophobicity.

For the larger tubes the behavior is distinct. For nanopores with  $a = 5.0$ , shown in the figure 3(b), the flow follows what was observed by Goldsmith and Martens [40] for TIP3P water confined in nanopores. The water-like fluid confined in pure solvophobic pore has a larger flow when compared with the pure solvophilic pore. However, this behavior is not linear with  $\phi$  but has a minimum. In order to understand the difference between the behavior at small and large  $a$  a more detail analysis of the structure of the liquid inside the tube was performed.

Previous studies have showed that the dynamical and structural properties of confined anomalous fluids are strongly correlated [21, 32]. Simulations with a high density for the fluid in the source reservoir and a similar TLS potential shows that in the narrowest nanopore,  $a = 1.75$ , the fluid is structured as a single file. As the nanotube radius is increased, more layers are observed, until the limit of large diameters and a bulk-like behavior [32]. In order to understand the distinct flow patterns with different nanopore radius the density and the fluid structure inside each nanopore were analyzed. The density profile was evaluated in the axial direction  $x$  and in the radial direction,  $r_\rho = (y^2 + z^2)^{1/2}$ , and then normalized accordingly with

$$\rho_{\text{normalized}}(\zeta) = \frac{\rho(\zeta)}{\int \rho(\zeta) d\zeta},$$



with  $\zeta = x$  or  $\zeta = r_\rho$  for axial and radial density profile, respectively.

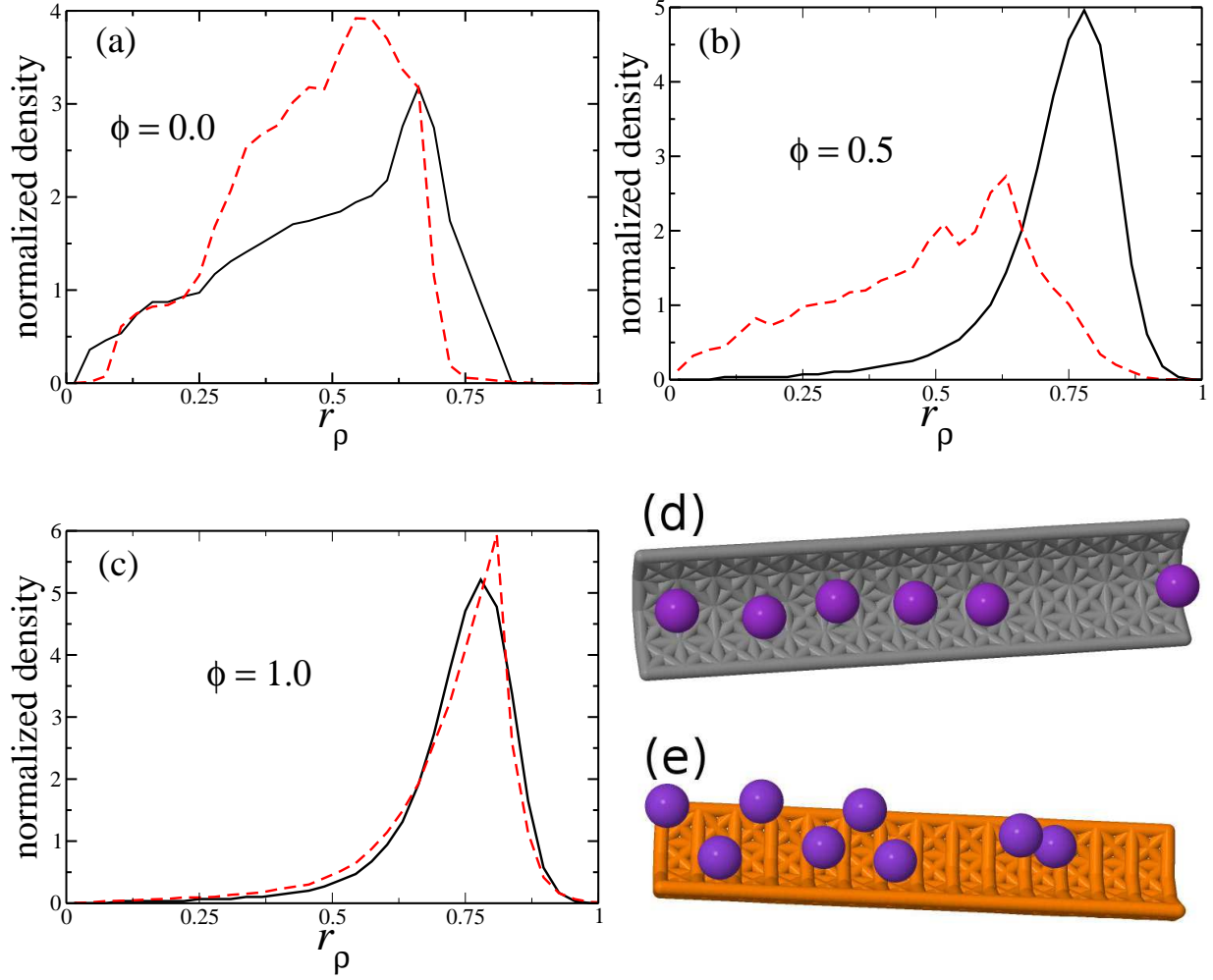


FIG. 4. Normalized density profile inside the nanopore with radius  $a = 1.75$  as function of the radial distance  $r_\rho$  near the entrance (solid black line) and near the exit (dashed red line) of the nanopore cavity, for nanopores with (a)  $\phi = 0.0$ , (b)  $\phi = 0.5$  and (c)  $\phi = 1.0$ . Snapshots showing the fluid inside the nanopore for the purely solvophobic (d) and purely Solvophilic (e) cases.

The radial density profile near the entrance and near the exit of the nanopore illustrates the differences between the flow for  $a = 1.75$  and for  $a = 5$ . The figure 4 shows that for functionalized pores with  $a = 1.75$  and (a) $\phi = 0.0$ , (b) $\phi = 0.5$  and (c) $\phi = 1.0$  the fluid is structured in a single layer. For  $\phi = 0.0$ , the solvophobic nanopore, the structure of the fluid at the entrance and at the exit are the same, with the fluid occupying a wide range of radial positions. For purely solvophilic nanopores,  $\phi = 1.0$ , the structure is also the same at the entrance and at the exit. The fluid, however, assumes a narrow distribution actually forming

a single line as shown in the figure 4(c). For nanopores partially solvophilic and partially solvophobic, as  $\phi = 0.5$  shown in the figure 4(b), two distinct behaviors were obtained. Near the entrance, where the solvophilic sites are located, the fluid forms a narrow single line, while at the exit, where the nanopore is solvophobic, the fluid occupies a wider range of positions in the radial direction. To clarify this structures, we show in figure 4(d) the snapshot for the purely solvophobic nanopore and in figure 4(e) for the purely solvophilic case. The narrow distribution of positions of this single line allows for the huge flow observed in solvophilic walls.

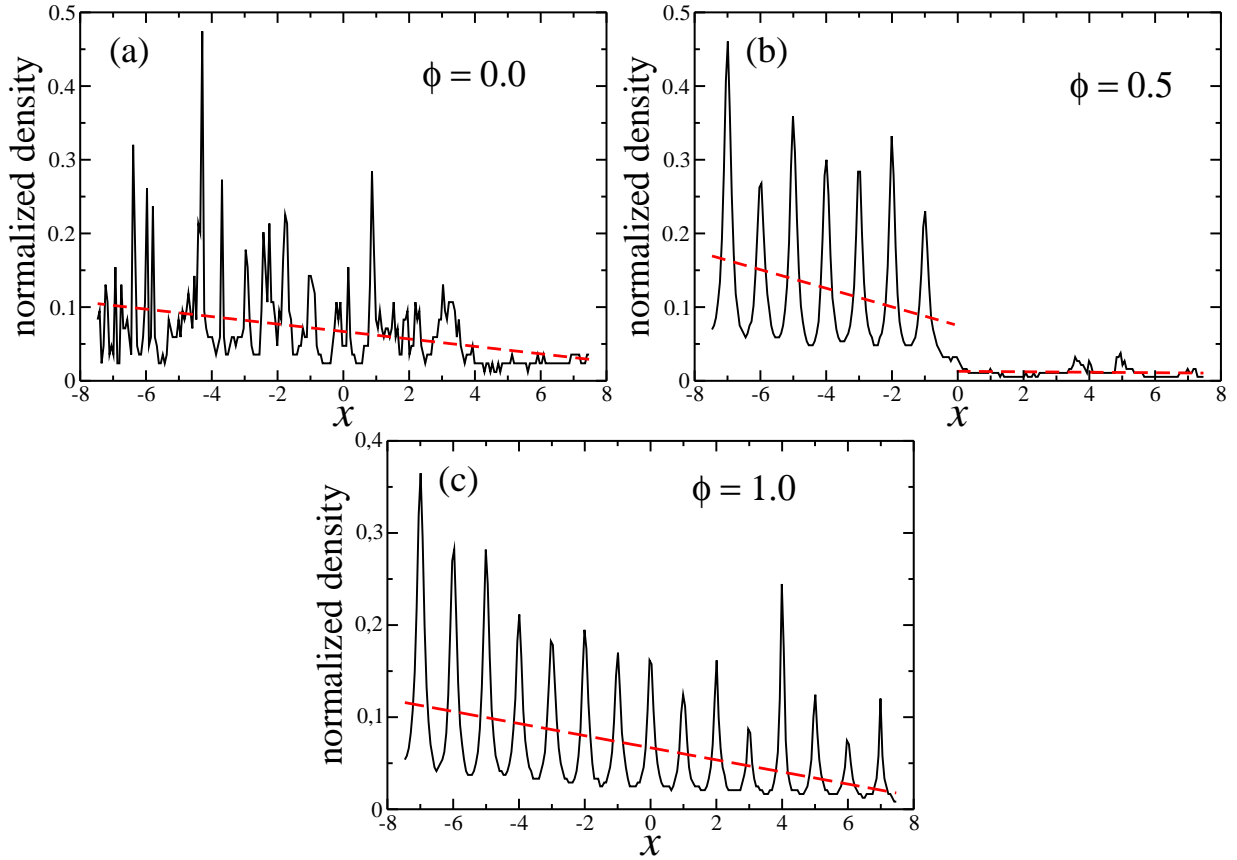


FIG. 5. Normalized density profile inside the nanopore as function of the axial direction  $x$ , for nanopores with radius  $a = 1.75$  (a)  $\phi = 0.0$ , (b)  $\phi = 0.5$  and (c)  $\phi = 1.0$ . The dashed red lines are the linear fits.

In the figure 5(a) the normalized density profile in the axial direction for narrow solvophobic nanopores is illustrated. The profile indicates a fluid without structure in the  $x$ -direction. The combination of the figure 5(a) with the figure 4(a) indicates that the fluid is in a low

density fluid phase. The dashed line in the figure 5(a) is a linear fit from the curve. For solvophobic walls fewer particles enter in the tube and their flow is not equally spaced. The decay indicates a density gradient inside the nanopore.

The solvophilic case, shown in the figure 5(c), the fluid exhibits a layered structure in the  $x$ -direction due to the interaction with the wall. Each peak in the figure 5(a) corresponds to the particles in the snapshot, Figure 4(e). Two length scales fluids tend to assume structures in the first or in the second length scale. In the confined case, the distance between the layers is approximately the particle radius. This is the first length scale in the potential defined by the Eq. 2. The linear fit in the  $\rho(x)$  curve also shows the existence of a density gradient in the nanopore. Then, in a solvophilic nanopore the fluid particles are arranged in the zig-zag single file layered structure, moving from one preferable distance to another. This more rigid structure in zig-zag moves faster than the disordered structure observed in the case of the solvophobic confinement.

In a partially solvophilic, partially solvophobic nanopore the two distinct structural behaviors in the  $x$ -direction are observed. The solvophilic region is a high density, well structured fluid, while in the solvophobic region there is a low density, non structured fluid, as the figure 5(c) shows. The linear fit in the structured region shows a high slope. Comparing with the Fick's Law for a one dimensional flow,  $J = -D(d\rho/dx)$  , where  $D$  is the diffusion coefficient, we can see that a higher slope will lead to a higher flow, which can easily leak through the solvophobic region. Therefore, the mixture of solvophilic and solvophobic sites plays a important role in the flow. In this way, the fluid flow increases when solvophilic sites are added to the nanopore until the threshold. This picture is quite similar to the description of Moskowitz et al [37] and Hummer et al [41].

Now, let us exam how is the density profile near the entrance and near the exit of the nanopore for  $a = 5$ . The figures 6(a) and (c) show the normalized density as a function of the radial distance in the case of purely solvophobic nanotube for the external forces  $f = 0.0$  and  $f = 0.05$ , respectively. In both cases the fluid does not show a well defined structure, with a fluid-like profile. No layering is observed and therefore not friction between the layers is observed. The figures 6(b) and (d) show the radial density profile for purely solvophilic nanopores for  $f = 0.0$  and  $f = 0.05$  respectively. Both near the entrance and at the end of the nanotube layering is observed with the contact layering showing a high density that increases at the end of the tube. The distance between layers corresponds to the

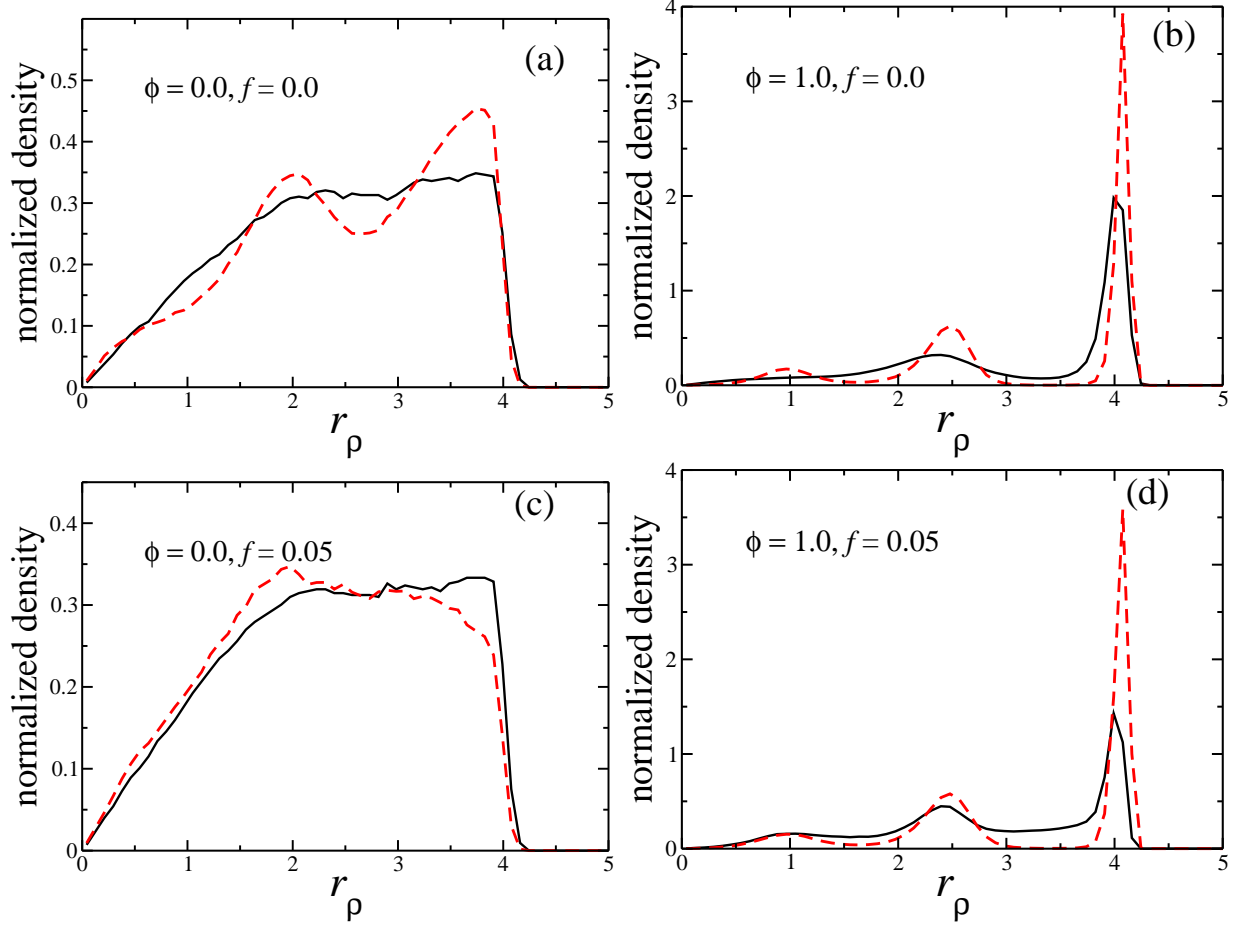


FIG. 6. Normalized density profile inside the nanopore with  $a = 5.0$  as function of the radial distance  $r_\rho$  near the entrance (solid black line) and near the exit (dashed red line) of the nanopore cavity, for nanopores with (a)  $\phi = 0.0$  and  $f = 0.0$ , (b)  $\phi = 1.0$  and  $f = 0.0$ , (c)  $\phi = 0.0$  and  $f = 0.05$  and (d)  $\phi = 1.0$  and  $f = 0.05$ .

second length scale what suggests that the system becomes quite stable in this configuration, making hard for the particles to move. This results is confirmed by the normalized axial density as a function of  $x$  illustrated in the figure 7. For the pure solvophobic system the density is uniform not indicating any organization, liquid-like. For the pure solvophilic, the system form a periodic structure what suggests almost a solid-like system [39, 40].

Then we can understand how the results of indicating that flow for solvophobic walls are faster [39, 40] are not contradictory to the results indicating that the flow for solvophilic walls are more rapid [37, 41]. In the first case [39, 40] the system well defined layers with the fluid wall particles being fully commensurated, in the second case either just a single layer

is formed or the flow is structured because wall-fluid are not commensurated [37, 41].

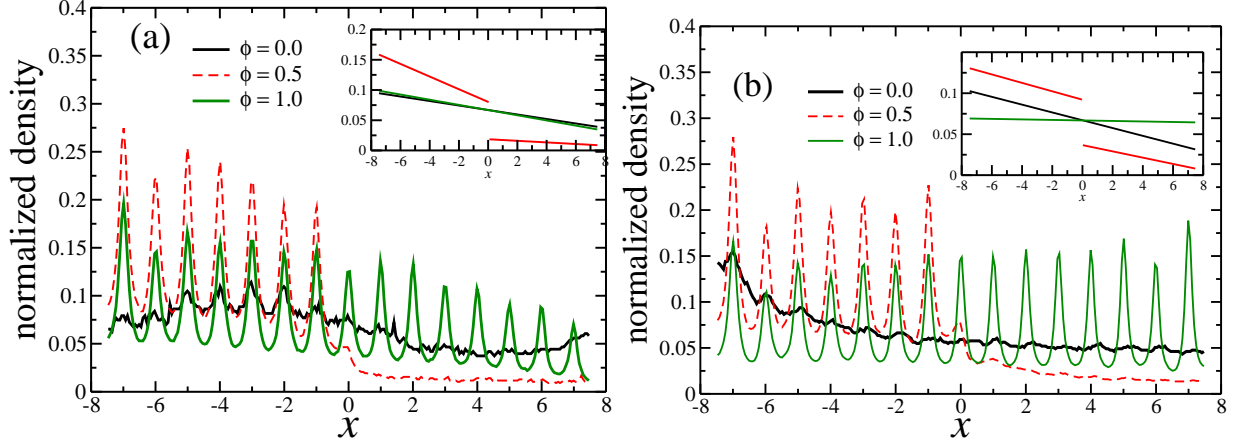


FIG. 7. Normalized density profile inside the nanopore as function of the axial direction  $x$ , for nanopores with radius  $a = 5.0$  (a)  $f = 0.0$  and (b)  $f = 0.05$ .

## B. Lennard-Jones-like Fluid

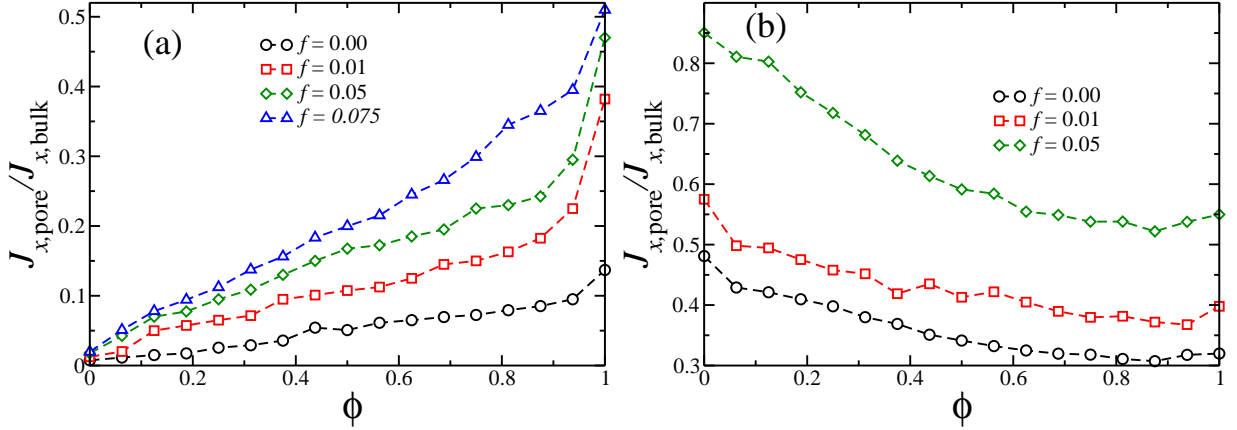


FIG. 8. Flux of non anomalous particles through the nanopore,  $J_{x,\text{pore}}$ , in units of the non-confined flux,  $J_{x,\text{bulk}}$ , as function of the fraction of solvophilic sites  $\phi$  for different external forces  $f$  and for cylindrical nanopores with radius (a)  $a = 1.75$  and (b)  $a = 5.00$ .

Next, we analyze if the flow in the system in which only one length scale is present differs from the flow in the two length scale system what could explain the difference between the flow of water and the flow of gases.

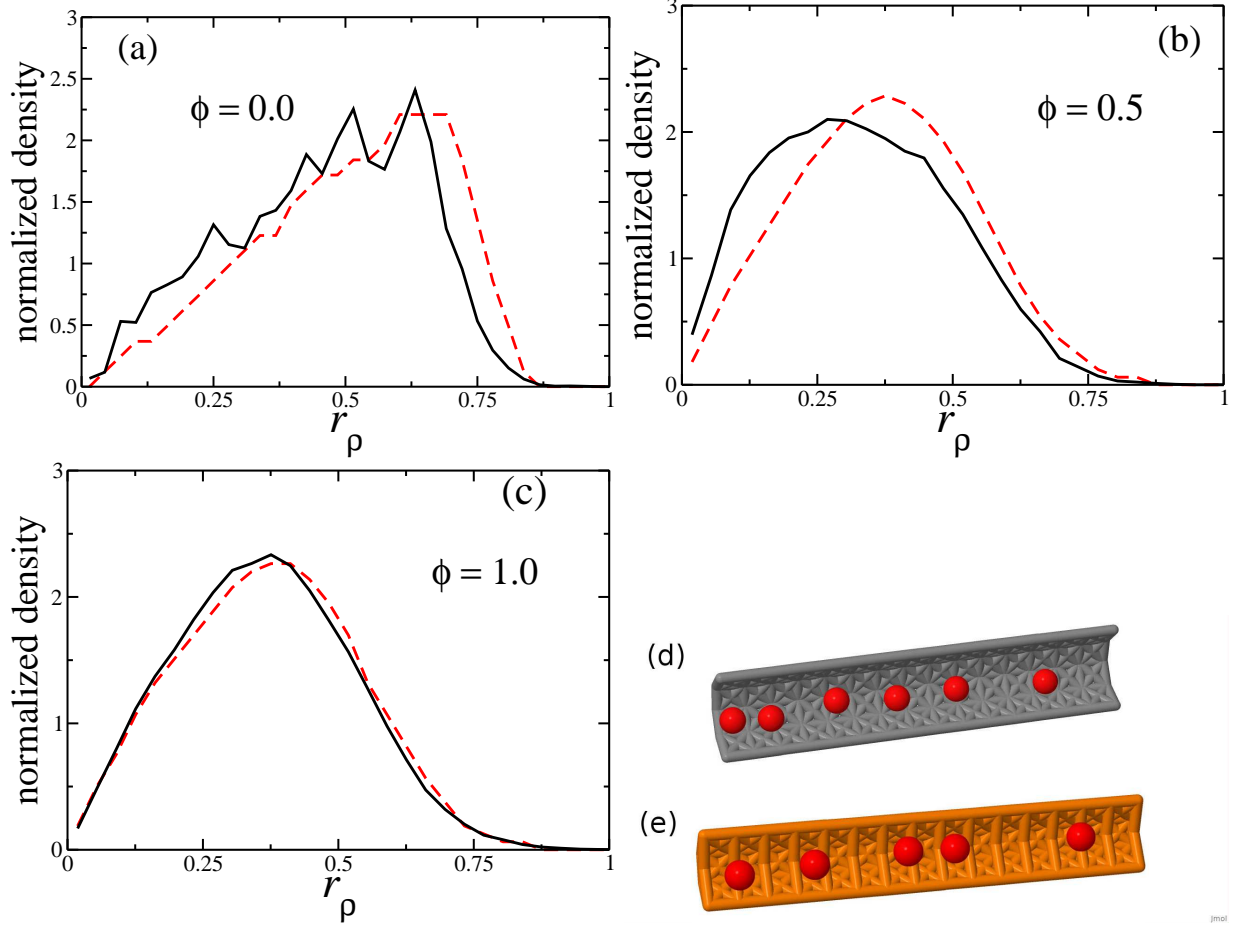


FIG. 9. Normalized density profile for the non anomalous fluid confined in a nanopore with radius  $a = 1.75$  as function of the radial distance  $r_\rho$  near the entrance (solid black line) and near the exit (dashed red line) of the nanopore cavity, for nanopores with (a)  $\phi = 0.0$ , (b)  $\phi = 0.5$  and (c)  $\phi = 1.0$ . Snapshots for the solvophobic (d) and solvophilic (e) cases.

The figures 8(a) and (b) illustrates the normalized flow for the LJ fluid for (a)  $a = 1.75$  and (b)  $a = 5$  respectively. The comparison of the figure 3 with the figure 8 shows that for both TLS and OLS potentials the flow is larger for the solvophilic when compared with the hydrophobic confinement. The mechanism for the increase of the flow with solvophilicity is the increase in density as the solvophilic confinement allow for more particles to enter into the tube [41]. This line, however, as illustrated in the figure 10 is not the same for the different types of confinement. For the solvophilic confinement the line is more organized and the particles in this single line move in jumps from one structure to the other. Since one line is present this movement shows almost no friction and the particles move faster in

the organized structure (solvophilic) than in the disorganized (solvophobic) arrangement.

The difference between the water-like and the LJ systems is the amount of flow that is higher for the TLS potential in the case of very small confinement, namely  $a = 1.75$ . This result that is consistent with experimental observations [27, 28] can be understood as follows is observed comparing the figure 3(a) with the figure 8(a). In the case of the TLS potential the single line is more compact as can be seen by comparing the figures 4 and 5 with the figures 9 and 10 since the two length scales allows for more mobility.

The difference between the TLS and OLS is also observed for  $a = 5$  case. While for the TLS the system forms layers, in the OLS no layer is observed as shown in the figure 11. This difference, however, does not impact the decrease in flux as the system becomes more solvophilic. This as in the case of the TLS potential results from our choice of particles that a commensurated with the wall. Then, as the system becomes more solvophilic the fluids organize on the wall forming a layer that increases friction.

#### IV. CONCLUSION

In this paper we addressed two questions related to the flow of fluids under nanoconfinement. First, we showed that the flow increase related to the change from solvophobic to solvophilic only happens if the particles and wall are not commensurated or if the flow occurs in a single line, what favors decorrelation with the wall. This effect is observed both for water-line and LJ type of flow.

Then, we compared the flow of water-like with LJ line fluid in order to understand the reason behind the faster flow of water when compared with non anomalous fluids as gases. Our results indicates that water-like fluids employ the two length scales to form more compact structures decreasing friction and allowing for a faster mobility.

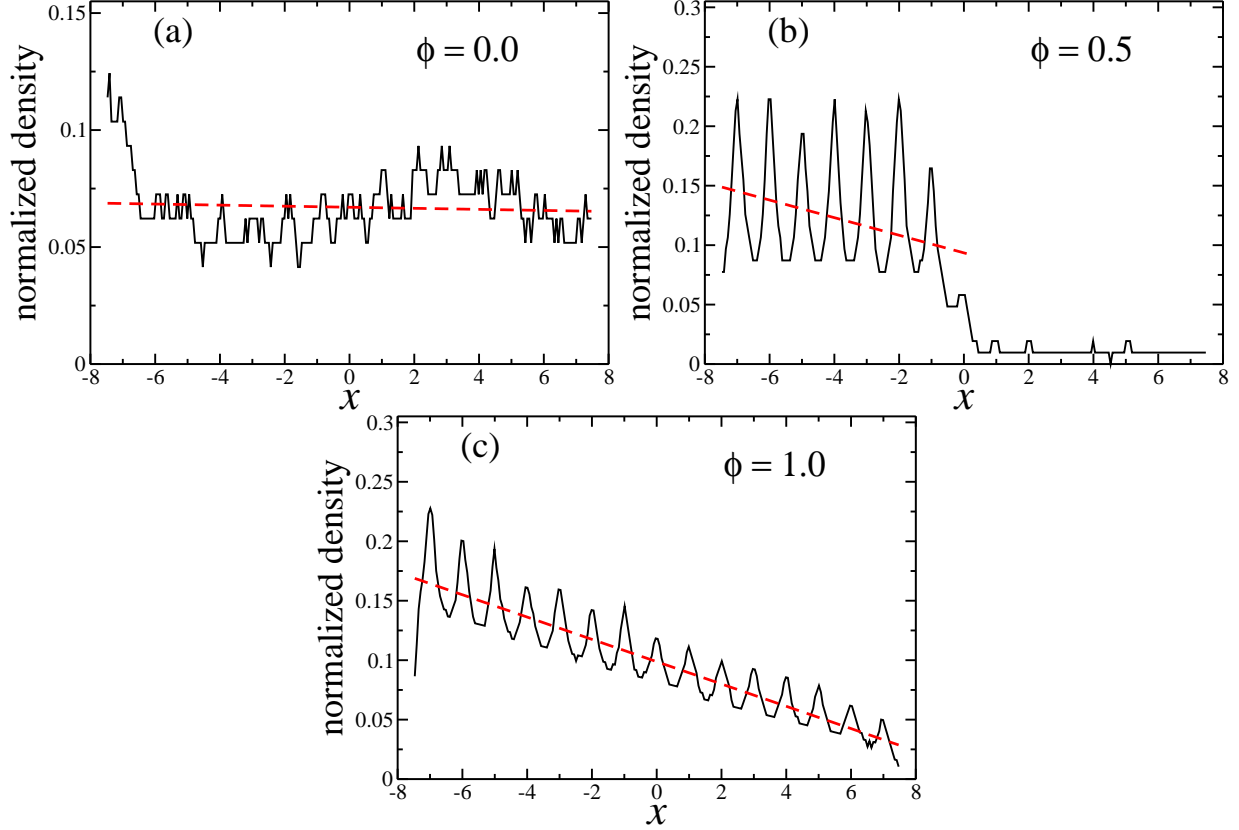


FIG. 10. Normalized density profile inside the nanopore as function of the axial direction  $x$ , for nanopores with radius  $a = 1.75$  (a)  $\phi = 0.0$ , (b)  $\phi = 0.5$  and (c)  $\phi = 1.0$ . The dashed red lines are the linear fits.

## V. ACKNOWLEDGMENTS

We acknowledge financial support from the Brazilian Agencies CNPq and FAPERGS.

- 
- [1] M. Chaplin, Seventh-three anomalies of water, <http://www.lsbu.ac.uk/water/anmlies.html>, 2014.
  - [2] P. A. Netz, F. W. Starr, M. C. Barbosa, and H. E. Stanley, *Physica A* **314**, 470 (2002).
  - [3] T. Morishita, *Phys. Rev. E* **72**, 021201 (2005).
  - [4] S. Sastry and C. A. Angell, *Nature Mater.* **2**, 739 (2003).
  - [5] G. S. Kellu, *J. Chem. Eng. Data* **20**, 97 (1975).
  - [6] R. Sharma, S. N. Chakraborty, and C. Chakravarty, *J. Chem. Phys.* **125**, 204501 (2006).



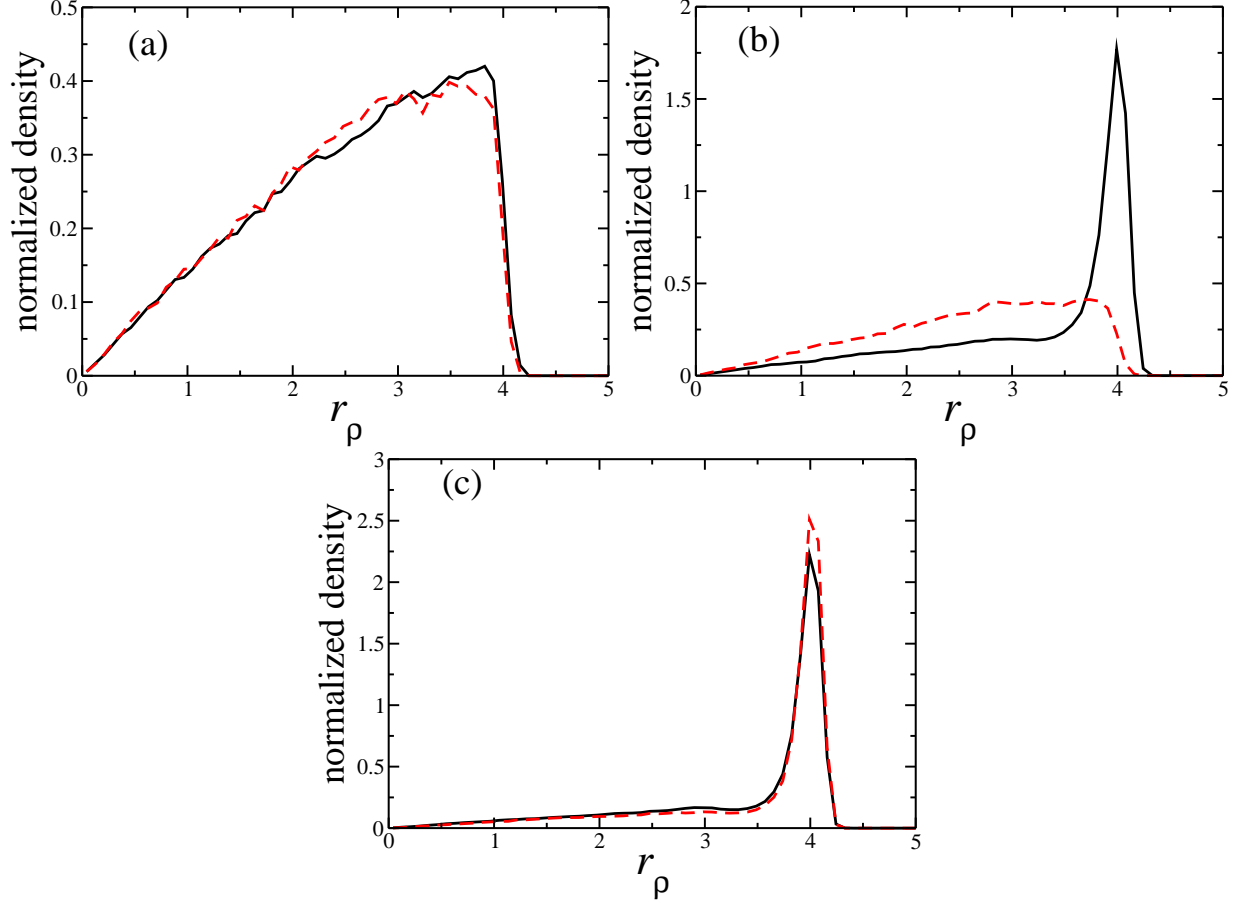


FIG. 11. Normalized density profile inside the nanopore with  $a = 5.0$  as function of the radial distance  $r_\rho$  near the entrance (solid black line) and near the exit (dashed red line) of the nanopore cavity, for

- [7] H. Thurn and J. Ruska, J. Non-Cryst. Solids **22**, 331 (1976).
- [8] *Handbook of Chemistry and Physics*, CRC Press, Boca Raton, Florida, 65 ed. edition edition, 1984.
- [9] S. J. Kennedy and J. C. Wheeler, J. Chem. Phys. **78**, 1523 (1983).
- [10] T. Tsuchiya, J. Phys. Soc. Jpn. **60**, 227 (1991).
- [11] P. T. Cummings and G. Stell, Mol. Phys. **43**, 1267 (1981).
- [12] M. Togaya, Phys. Rev. Lett. **79**, 2474 (1997).
- [13] C. A. Angell, R. D. Bressel, M. Hemmatti, E. J. Sare, and J. C. Tucker, Phys. Chem. Chem. Phys. **2**, 1559 (2000).

- [14] G. Malescio, G. Franzese, A. Skibinsky, S. V. Buldyrev, and H. E. Stanley, Phys. Rev. E **71**, 061504 (2005).
- [15] E. A. Jagla, Phys. Rev. E **58**, 1478 (1998).
- [16] A. Scala, F. W. Starr, E. La Nave, F. Sciortino, and H. E. Stanley, Nature (London) **406**, 166 (2000).
- [17] L. Xu et al., Proc. Natl. Acad. Sci. U.S.A. **102**, 16558 (2005).
- [18] A. B. de Oliveira, P. A. Netz, T. Colla, and M. C. Barbosa, J. Chem. Phys. **124**, 084505 (2006).
- [19] Y. D. Fomin, E. N. Tsiok, and V. N. Ryzhov, J. Chem. Phys. **135**, 234502 (2011).
- [20] L. Krott and M. C. Barbosa, J. Chem. Phys. **138**, 084505 (2013).
- [21] L. Krott and J. R. Bordin, J. Chem. Phys. **139**, 154502 (2013).
- [22] L. Krott and M. C. Barbosa, Phys. Rev. E **89**, 012110 (2014).
- [23] J. R. Bordin, L. Krott, and M. C. Barbosa, J. Phys. Chem. C **118**, 9497 (2014).
- [24] J. R. Bordin, L. B. Krott, and M. C. Barbosa, J. Chem. Phys. **141**, 144502 (2014).
- [25] L. B. Krott, J. R. Bordin, and M. C. Barbosa, J. Phys. Chem. B **119** (2015).
- [26] L. B. Krott, J. R. Bordin, N. M. Barraz Jr, and M. C. Barbosa, J. Chem. Phys. **142** (2015).
- [27] J. K. Holt et al., Science **312**, 1034 (2006).
- [28] X. Qin, Q. Yuan, Y. Zhao, S. Xie, and Z. Liu, Nanoletters **11**, 2173 (2011).
- [29] J. A. Thomas and A. J. H. Macgaughey, Phys. Rev. Lett. **102**, 4502 (2009), 18.
- [30] S. Roy, M. Bhadra, and S. Mitra, Separation and Purification Technology **136** (2014).
- [31] J. R. Bordin, A. B. de Oliveira, A. Diehl, and M. C. Barbosa, J. Chem. Phys **137**, 084504 (2012).
- [32] J. R. Bordin, A. Diehl, and M. C. Barbosa, J. Phys. Chem. B **117**, 7047 (2013).
- [33] J. R. Bordin, J. S. Soares, A. Diehl, and M. C. Barbosa, J. Chem Phys. **140**, 194504 (2014).
- [34] V. V. Chaban and O. V. Prezhdo, ACS Nano **8** (2014).
- [35] M. Majumder, N. Chopra, and B. J. Hinds, ACS Nano **5** (2011).
- [36] H. Yasuoka, R. Takahama, M. Kaneda, and K. Suga, Phys. Rev. E **92** (2015).
- [37] I. Moskowitz, M. A. Snyder, and J. Mittal, J. Chem. Phys. **141** (2014).
- [38] N. Giovambattista, P. J. Rossky, and P. G. Debenedetti, J. Phys. Chem. B **113**, 13723 (2009).
- [39] Y. Liu, W. Li, T. Perez, J. D. Gunton, and G. Brett, Langmuir **28** (2012).
- [40] J. Goldsmith and C. C. Martens, Phys. Chem. Chem. Phys. **11** (2009).

- [41] G. Hummer, J. C. Rasaiah, , and J. P. Noworyta, *Nature (London)* **414**, 188 (2001).
- [42] N. G. Chopra et al., *Science* **269**, 966 (1995).
- [43] X. Wei, M.-S. Wang, Y. Bando, and D. Golberg, *J. Am. Chem. Soc.* **132**, 13592 (2010).
- [44] S. H. Barghi, T. T. Tsotsis, and M. Sahimi, *International Journal of Hydrogen energy* **41**, 369 (2016).
- [45] J. Jin, L. Fu, H. Yang, and J. Ouyang, *Scientific Reports* **5**, 12429 (2015).
- [46] P. Allen and D. J. Tildesley, *Computer Simulation of Liquids*, Oxford University Press, Oxford, 1987.
- [47] P. G. Debenedetti, V. S. Raghavan, and S. S. Borick, *J. Chem. Phys.* **95** (1991).
- [48] G. S. Heffelfinger and F. Van Smol, *J. Chem. Phys.* **100**, 7548 (1994).
- [49] J. R. Bordin, A. Diehl, M. C. Barbosa, and Y. Levin, *Phys. Rev. E* **85**, 031914 (2012).